Enhancing bifunctional and overall water splitting electrocatalytic activity copper MOF by integrating conducting rGO

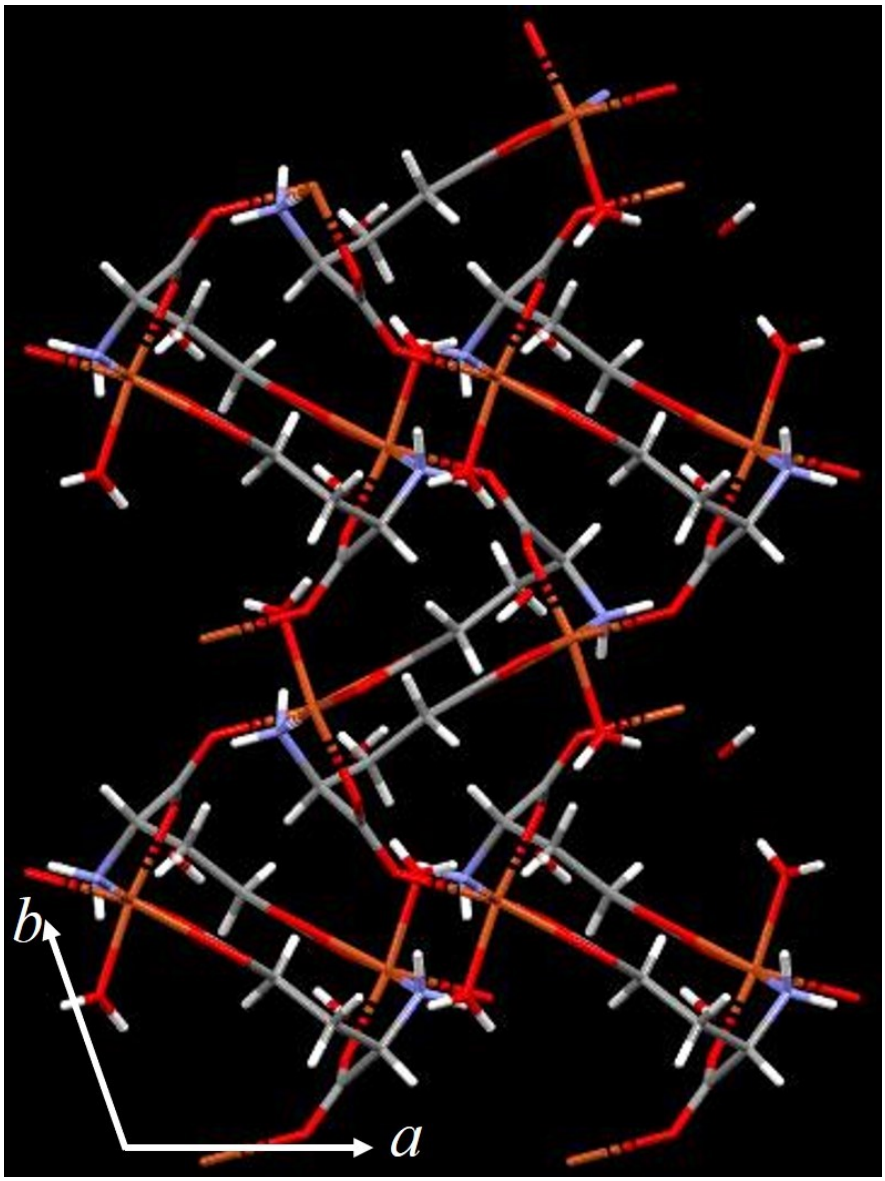

Figure S1. Molecular packing in the crystal lattice of CuMSG.

Table S1. Crystal data and structure refinement for CuMSG.

Empirical formula	C5 H11 Cu N O6	
Formula weight	244.69	
Temperature	220(2) K	
Wavelength	0.600 Å	
Crystal system	Orthorhombic	
Space group	$P2_12_12_1$	
Unit cell dimensions	a = 7.1900(14) Å	α = 90°
	b = 10.237(2) Å	β = 90°
	c = 10.987(2) Å	γ = 90°
Volume	808.7(3) $Å^3$	
Z	4	
Density (calculated)	2.010 Mg/m^3	
Absorption coefficient	1.701 mm^{-1}	
F(000)	500	
Crystal size	0.104 x 0.098 x 0.087 mm^3	
Theta range for data collection	2.296 to 24.993°.	
Index ranges	-10<=h<=10, -14<=k<=14, -15<=l<=15	
Reflections collected	8747	
Independent reflections	2371 [R(int) = 0.0982]	
Completeness to theta = 21.100°	99.5 %	
Absorption correction	Empirical	
Max. and min. transmission	1.000 and 0.948	
Refinement method	Full-matrix least-squares on F^2	
Data / restraints / parameters	2371 / 10 / 131	
Goodness-of-fit on F^2	1.084	
Final R indices [I>2sigma(I)]	R1 = 0.0298, wR2 = 0.0706	
R indices (all data)	R1 = 0.0298, wR2 = 0.0707	
Absolute structure parameter	-0.009(5)	
Extinction coefficient	0.090(7)	
Largest diff. peak and hole	0.658 and -1.184 $e \cdot Å^{-3}$	

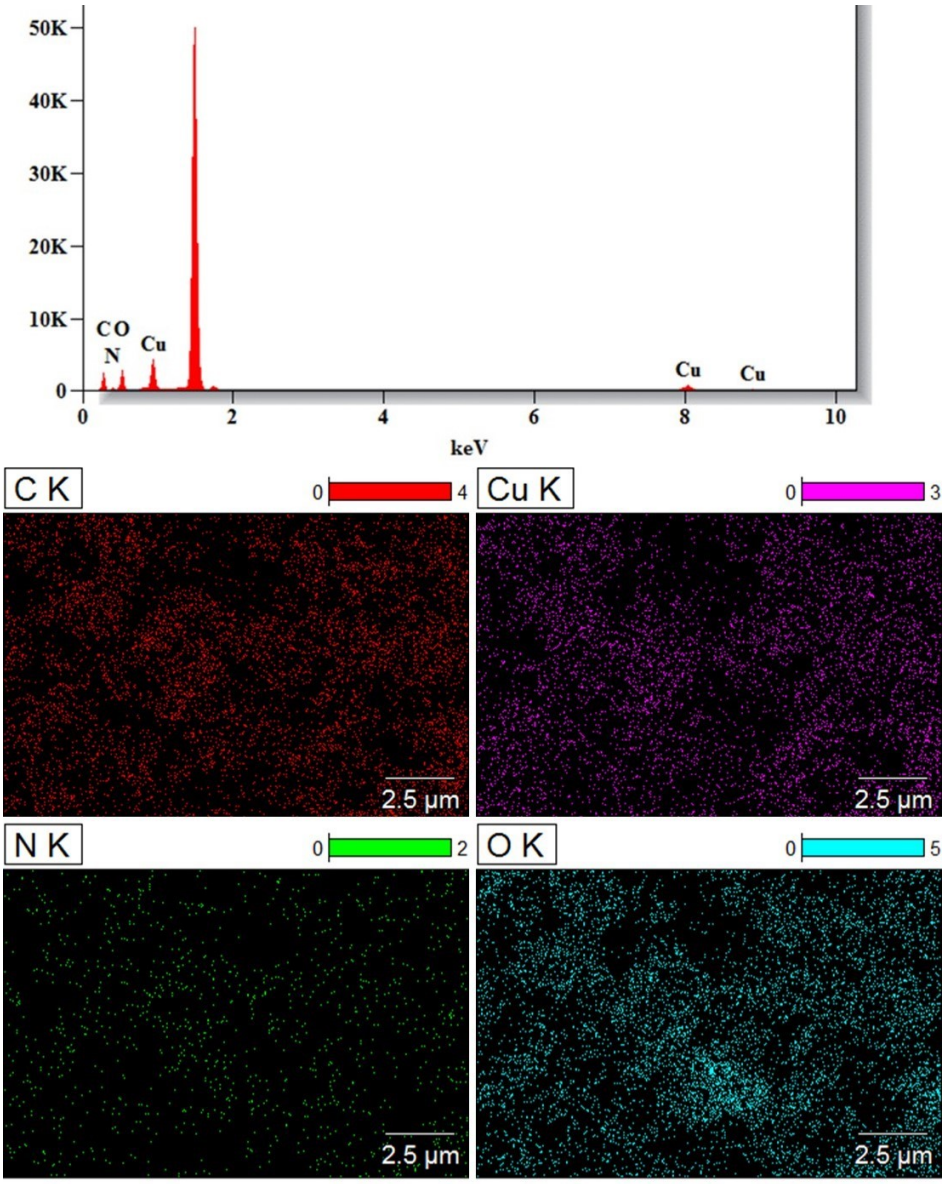

Figure S2. EDX spectrum (top) and elemental mapping (bottom) of CuMSG.

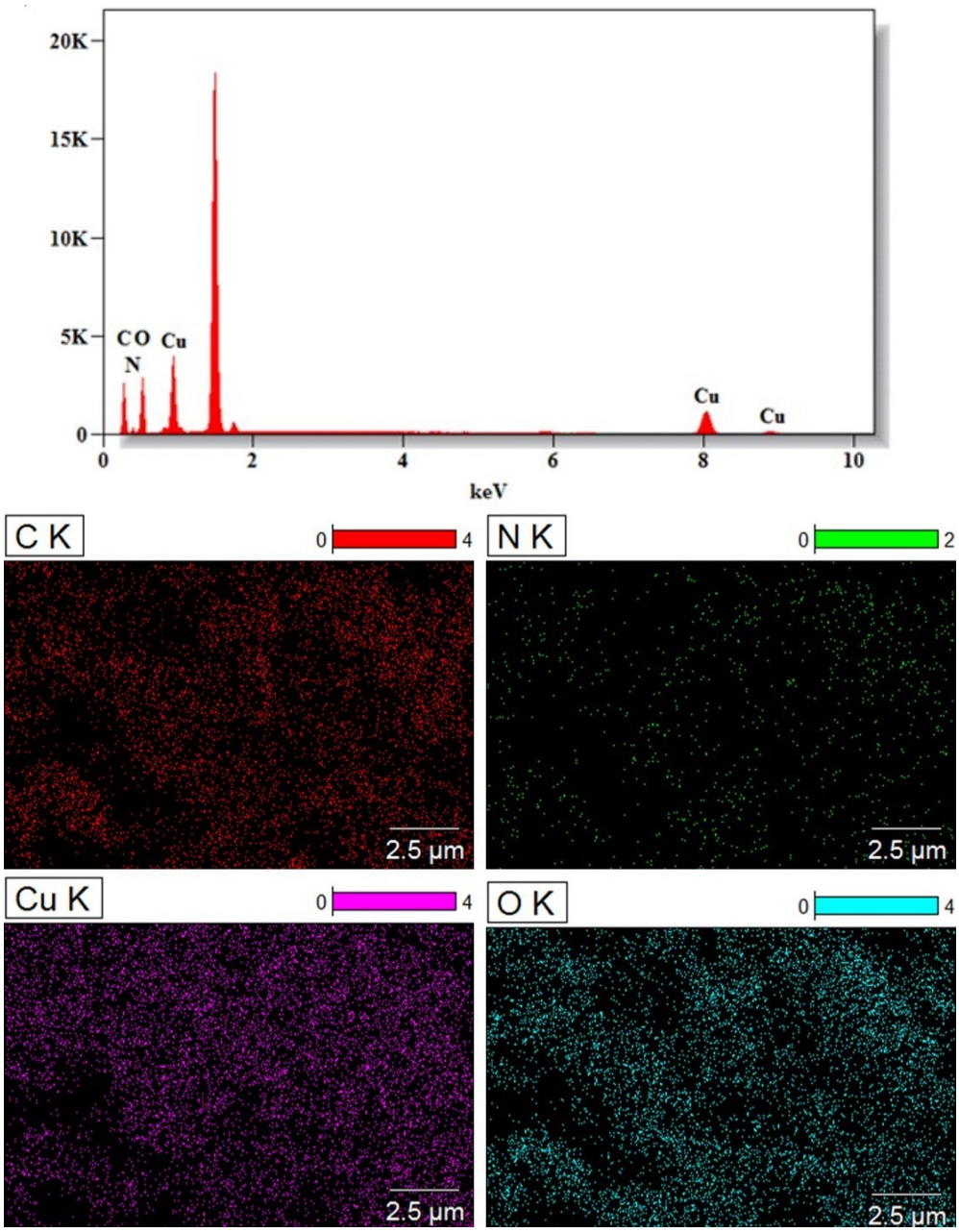

Figure S3. EDX spectrum (top) and elemental mapping (bottom) of CuMSG/rGO.

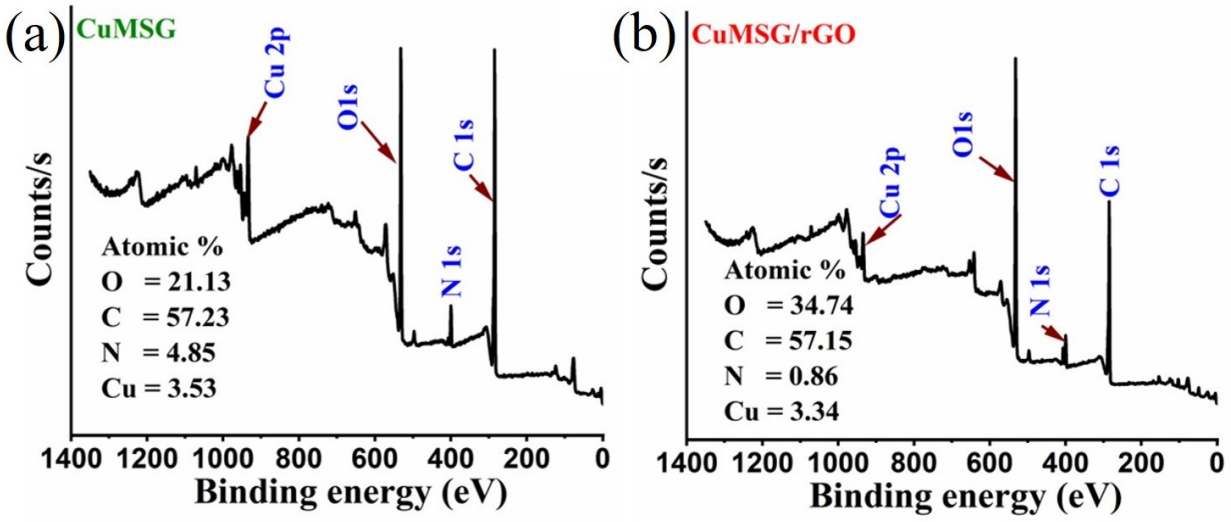

Figure S4. XPS survey spectra of (a) CuMSG and (b) CuMSG/rGO.

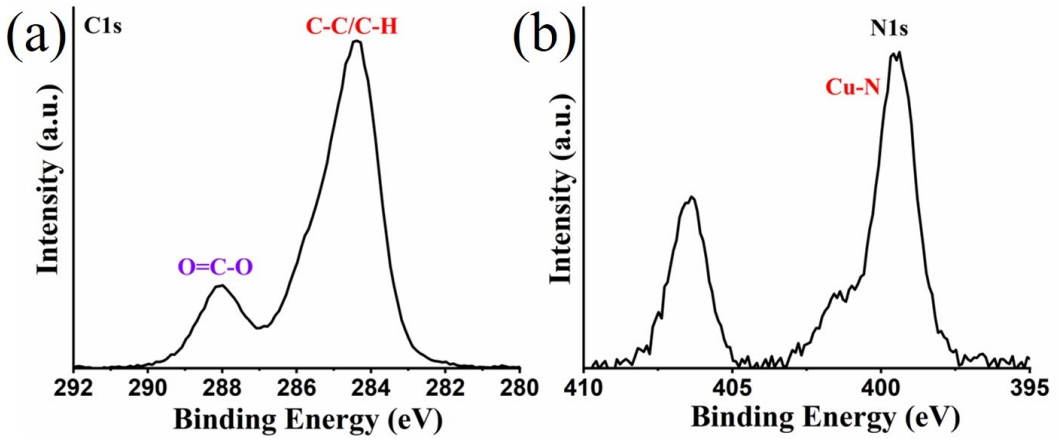

Figure S5. High resolution XPS spectra of (a) C1s and (b) N1s of CuMSG/rGO composite.

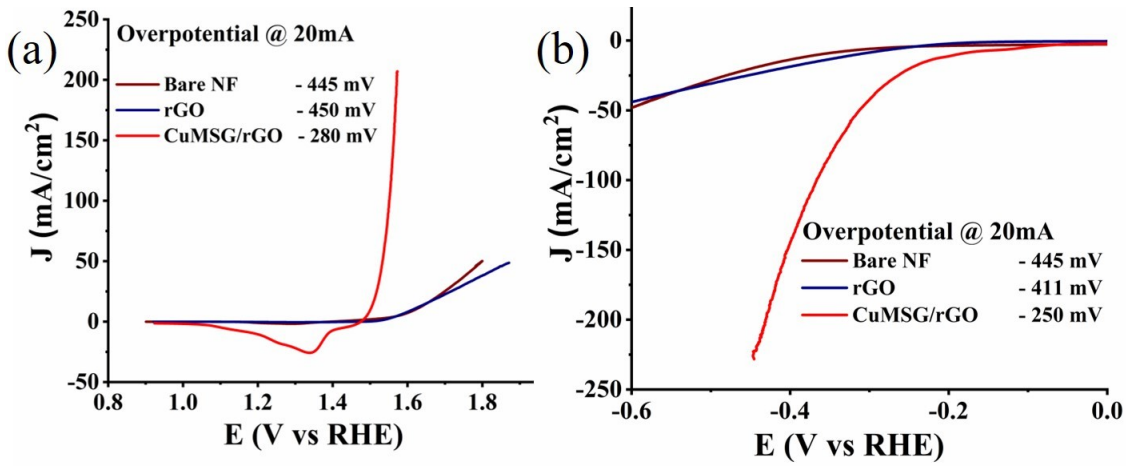

Figure S6. Comparison of (a) OER and (b) HER polarization curve of CuMSG/rGO composite with bare NF and rGO coated NF.

Figure S7. Electrochemical impedance spectra of (a) OER, (b) HER and (c) overall water splitting using CuMSG and CuMSG composites.

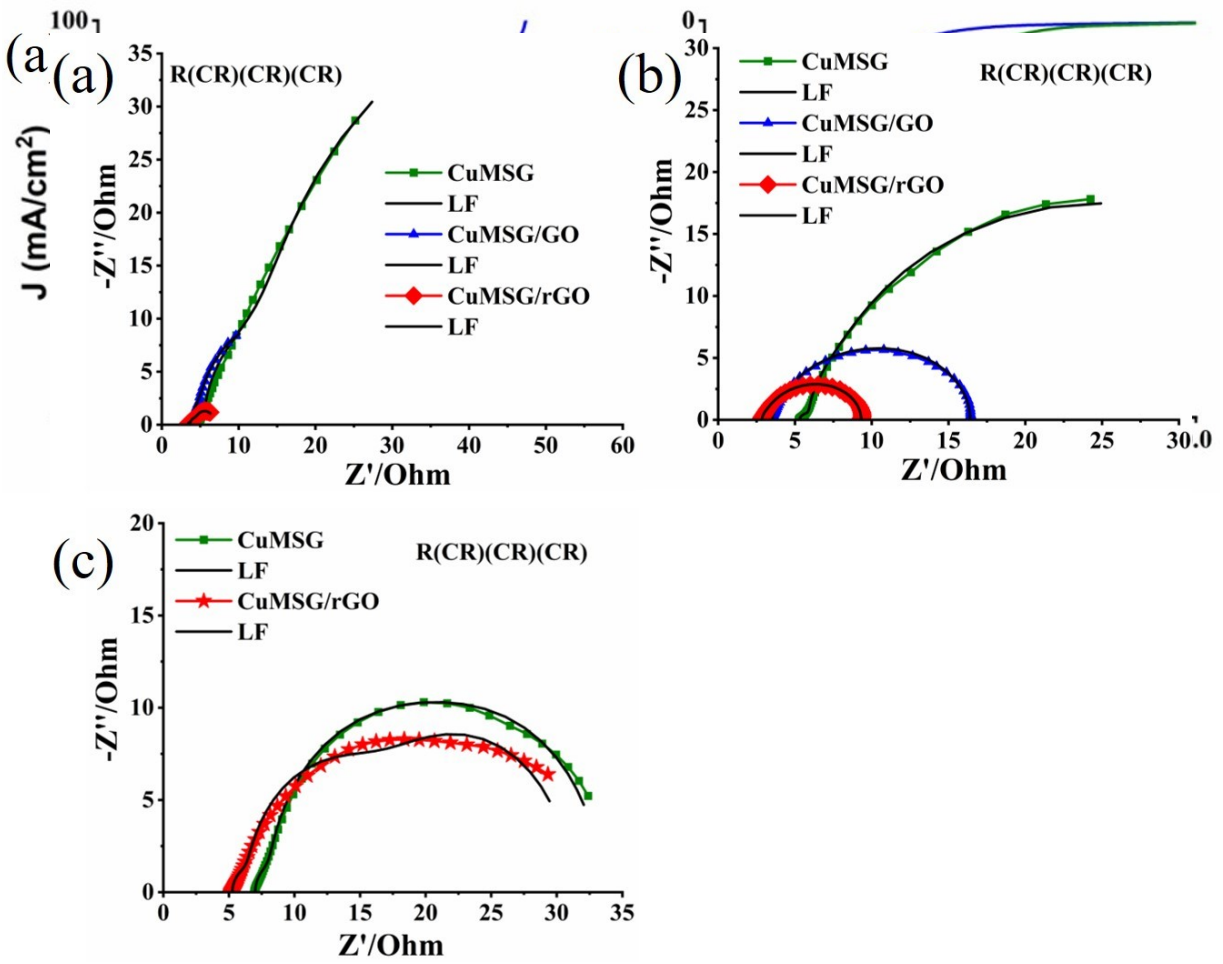

Figure S8. (a) OER and (b) HER polarization curve of CuMSG/rGO composite before and after stability test.

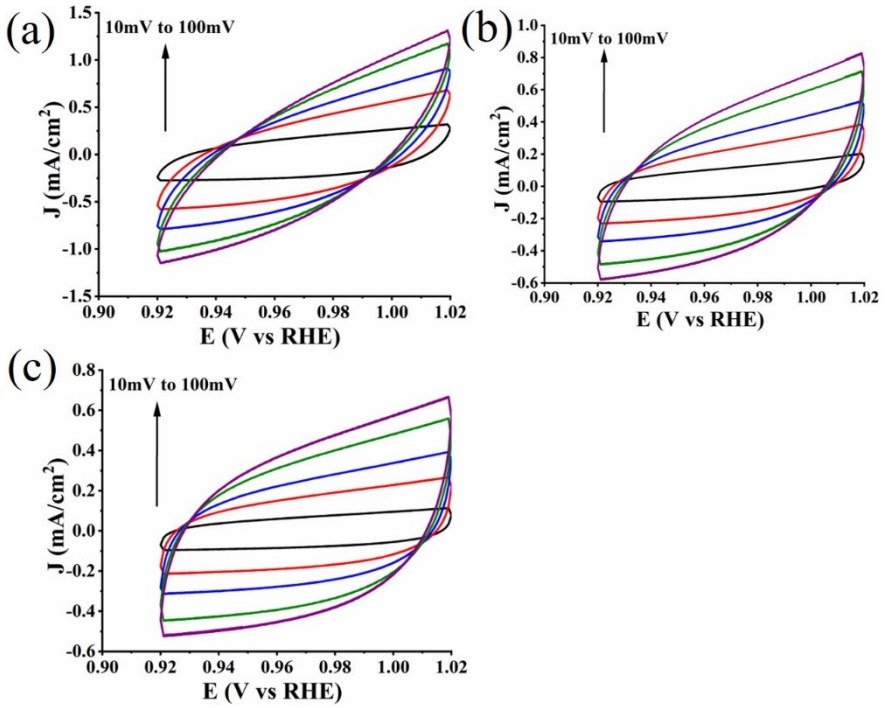

Figure S9. Double layer capacitance and capacitive currents as a functional of scan rate of (a) CuMSG, (b) CuMSG/GO and (c) CuMSG/rGO.

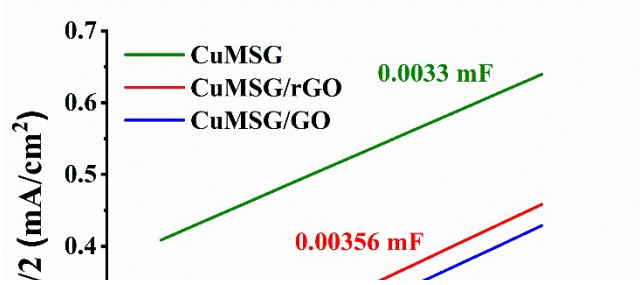

Figure S10. Linear relationship between ΔJ/2 vs Scan rate ν.

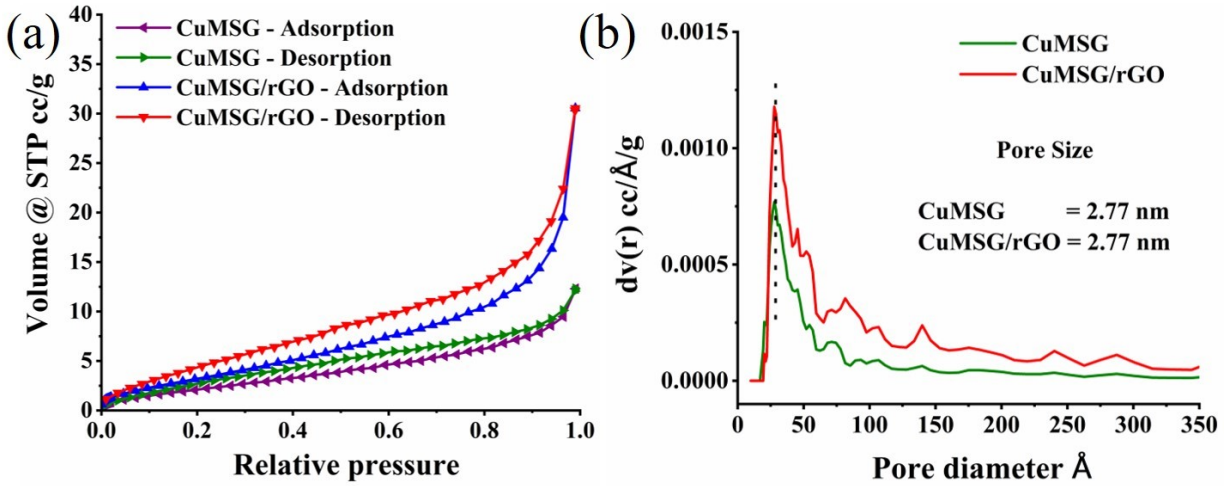

Figure S11. BET (a) adsorption/desorption isotherm and (b) pore diameter analysis of CuMSG and CuMSG/rGO.

Table S2. Surface area analysis of CuMSG and CuMSG/rGO.

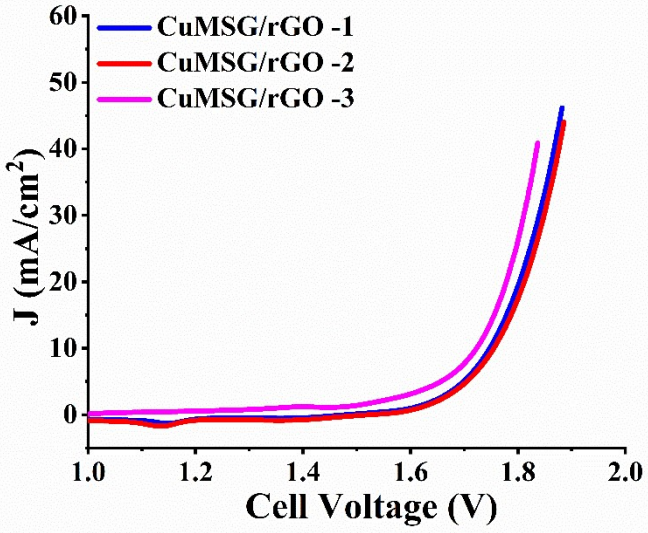

	BET surface area	Pore volume	Pore diameter
CuMSG	9.706 $m^2 g^{-1}$	0.015 cc g^{-1}	2.77 nm
CuMSG/rGO	14.964 $m^2 g^{-1}$	0.033 cc g^{-1}	2.77 nm

Figure S12. LSV curve of three different batch samples of CuMSG/rGO.

Table S3. Comparison of CuMSG MOF composites electrocatalytic activity with the previously reported materials. η = overpotential.

S.No	Material	OER		HER		Ref
		η (current density)	Tafel mV/dec	η (current density)	Tafel mV/dec	
1	CuMSG/rGO	280(20)	48	250(20)	128	This work
2	CuMSG/GO	299(20)	60	289(20)	169	This work
3	CuMSG	408(20)	75	381(20)	170	This work
4	Meso-Cu-BTC	NA	NA	89.32(6)	33.41	1
5	Fe_8Cu_2CN (PBAs)	290(10)	112	150(10)	118	2
6	Cu(I)	390(10)	180	700(10)	108	3
7	Cu(II)	300(10)	50	650(10)	90	3
8	copper paddle−wheel system	617(10)	116	NA	NA	4
9	$[Li(H_2O)_4]$-$[\{CuI(H_2O)1.5\}\{CuII(H_2O)_3\}_2\{WVI_{12}O_{36}(OH)6\}]\cdot N_2\cdot H_2S\cdot 3H_2O$	418	356.42	443	314.2	5
10	CPE-CuL	390(10)	192	NA	NA	6
11	CuFe(1:2)MOF	NA	NA	175	295	7
12	$Fe(OH)_x$@Cu-MOF NBs	NA	NA	112	76	8
13	Cu-MOF NPs	NA	NA	273	118	8
14	Cu@1 MOF	420(1)	-	NA	NA	9
15	CuMOF	463(10)	32.71	NA	NA	10
16	$Cu_3(HITP)_2$	600(10)	329.2	NA	NA	11

References

1 R. Nivetha, A. Sajeev, A. Mary Paul, K. Gothandapani, S. Gnanasekar, P. Bhardwaj, G. Jacob, R. Sellappan, V. Raghavan, K. C. N, S. Pitchaimuthu, S. K. Jeong and A. Nirmala Grace, *Mater. Res. Express*, 2020, **7**, 114001.

2 M. Sreenivasulu, R. S. Shetti, S. Mathi and N. P. Shetti, *Electrochimica Acta*, 2024, **492**, 144340.

3 C. S. A. Djadock, S. Vengatesan, K. Annamalai Sami, E. S. Mefouegang, A. Nana, J. Ngoune, S. Ravichandrana and S. Vasudevan, *J. Inorg. Organomet. Polym. Mater.*, DOI:10.1007/s10904-025-03854-w.

4 R. Mishra, E. Ülker and F. Karadas, *ChemElectroChem*, 2017, **4**, 75–80.

5 A. Ravi, S. Mulkapuri and S. K. Das, *Inorg. Chem.*, 2023, **62**, 12650–12663.

6 Z. Shaghaghi, P. S. Kouhsangini and R. Mohammad-Rezaei, *Appl. Organomet. Chem.*, 2021, **35**, e6103.

7 D. S. H. Kumar, M. A. Pandit, V. K. Kolakaluri and K. Muralidharan, *J. Environ. Sci.*, 2025, S1001074225002608.

8 W. Cheng, H. Zhang, D. Luan and X. W. (David) Lou, *Sci. Adv.*, 2021, **7**, eabg2580.

9 A. Goswami, D. Ghosh, V. V. Chernyshev, A. Dey, D. Pradhan and K. Biradha, *ACS Appl. Mater. Interfaces*, 2020, **12**, 33679–33689.

10 H. Hayat, T. Noor, N. Iqbal, R. Ahmed, N. Zaman and Y. Huang, *J. Environ. Chem. Eng.*, 2023, **11**, 109627.

11 M. Zhang, M. Liu, M. Yang, X. Liu, S. Shen, J. Wu and W. Pei, *J. Solid State Chem.*, 2023, **325**, 124133.